AUTO-ROI SYSTEM:AUTOMATIC LOCALIZATION OF ROI IN GIGAPIXEL WHOLE-SLIDE IMAGES

by

SHIRONG XUE

Presented to the Faculty of the Graduate School of
The University of Texas at Arlington in Partial Fulfillment
of the Requirements
for the Degree of

MASTER OF SCIENCE IN COMPUTER SCIENCE

THE UNIVERSITY OF TEXAS AT ARLINGTON
Arpil 2017

To my parents and my wife, for their endless trust, support, encouragement and love.

ACKNOWLEDGEMENTS

I would like to express my sincere gratitude to my supervising professor, Dr. Junzhou Huang for the continuous support of my Master's study and related research. Because of his motivation, friendly advice, and immense knowledge, I can successfully complete this thesis. His guidance helped me a lot in the whole process of thesis research, writing and defense. I sincerely express my gratitude to Dr. Junzhou Huang, Dr. Heng Huang, and Dr. Jia Rao for spending their valuable time by serving on my committee.

I would also like to extend my appreciation to Mr. Jiawen Yao, my P.hD mentor for his continuous assistance in this thesis and also I wish to mention special thanks to all the friends in the SMILE lab for constantly motivating me to achieve success and sharing their suggestions on every step in this project.

I would fail if I forget to express my gratitude to all the professors and advisors Mr. Bahram Khalili, Ms. Camille Costabile, Dr Chris Ding, Dr. Ramez Elmasri, Dr. Gergely Zaruba, Mr. Sajib Datta, Mr. John Robb, advisors in the Office of International Education and all my dear friends in Arlington and China for their boundless belief in my abilities and endless encouragement for my success.

Finally, I would like to express my deep gratitude to my wife and my parents, for their sacrifice, encouragement, and patience.

Arpil 19, 2017

ABSTRACT

AUTO-ROI SYSTEM:AUTOMATIC LOCALIZATION OF ROI IN GIGAPIXEL WHOLE-SLIDE IMAGES

Shirong Xue, M.S.

The University of Texas at Arlington, 2017

Supervising Professor: Junzhou Huang

Digital Pathology is a very promising approach to diagnostic medicine to accomplish better, faster prognosis and prediction of cancer. The high-resolution whole slide imaging (WSI) can be analyzed on any computer, easily stored, and quickly shared. However, a digital WSI is quite large, like over 106 pixels by 106 pixels (3TB), depending on the tissue and the biopsy type. Automatic localization of regions of interest (ROIs) is important because it decreases the computational load and improves the diagnostic accuracy. Some popular applications in the market already support in viewing and marking the ROIs, such as ImageScope, OpenSlide, and ImageJ. However, it only shows some regions as a result and is hard to learn pathologists' behavior for future research and education. In this thesis, we propose a new automatic system, named as Auto-ROI, to automatically localize and extract diagnostically relevant ROIs from the pathologists' daily actions when they are viewing the WSI. Analyzing action information enables researchers to study pathologists' interpretive behavior and gain a new understanding of the diagnostic medical decision-making process. We compare the ROIs extracted by the proposed system with the ROIs marked by Im-

ageScope in order to evaluate the accuracy. Experiment results show the Auto-ROI System can help to achieve a good performance in survival analysis.

TABLE OF CONTENTS

LIST OF ILLUSTRATIONS

LIST OF TABLES

CHAPTER 1

Introduction

Cancer is a major public health problem worldwide and is the second leading cause of death in the United States. In recent decades, Whole slide imaging technology has become the prevalent method for the cancer diagnosis. Annotating region of interests, segmentation, and detection are the necessary process of image analysis. A novel system is proposed in this thesis to automatically localize ROI[1, 2]. Compared with the existing system in the market, the new system improves the performance of the ROI localization and makes it possible to apply the pathologists behavior information to the future research and education.

1.1 Cancer

The incidence and mortality of cancer worldwide have increased steadily since last century. Also, there has also been an increasing growth in cancer cases within the United States. Typically, cancer causes cells to proliferate in an uncontrolled abnormal cell growth, thereby potential to spreading to other parts of the body.

1.2 Lung Cancer

Lung cancer is a malignant lung tumor characterized by uncontrolled outgrowth of a clonal population of cell in lung tissues[3]. The cancer cells can spread from the lung to other parts of the body through blood vessels and grow new tumors to threaten other tissues[4]. As researchers study indicates, lung cancer has already become to one of the four most prevalent cancers and accounts for 12% of all new

cases of cancers worldwide[5]. As the second most common cancer diagnosed in patients, it caused a significant cancer-related death in the United States. National Cancer Institute released the statistics data that the estimated lung cancer cases were 222,500 and the estimated death case was 155,870 in the United States this year[1]. This serious situation arouses people's attention and makes this disease become a concerned health-care issue in these years.

1.2.1 Types

There are two main categories of lung cancer: non-small cell lung cancer (NSCLC) and small cell lung cancer (SCLC). The Non-small cell lung cancer includes squamous cell carcinoma (also called epidermoid carcinoma), large cell carcinoma, adenocarcinoma, pleomorphic, carcinoid tumor, salivary gland carcinoma, and unclassified carcinoma. While the small cell lung cancer has small cell carcinoma (oat cell cancer) and combined small cell carcinoma[2].

1.2.2 Causes

Most of the lung cancer cases are a result of the popularity of cigarette smoking, outdoor and indoor air pollution, radon gas, genetic predispositions, modification or mutation of DNA/RNA, and so on. While the cigarette smoking is by far widely recognized as the most important risk factor of the causes of lung cancer. As research outcome shows that the long-term tobacco smoking is linked to more than 80% of all lung cancer cases in the United States and other countries where smoking is widespread[6].

[1]https://seer.cancer.gov/statfacts/html/lungb.html/

[2]https://seer.cancer.gov/statfacts/html/lungb.html/

1.2.3 Symptoms

Pain is one of the most common symptoms of patients that are diagnosed with lung cancer. They also have some signs and symptoms of cough, wheezing, losing weight, fatigue, weakness, fever, etc.

1.3 Computer-Aided Diagnosis

Computer-aided diagnosis (CAD) has become one of the major technique in medical imaging processing and disease image diagnosis. Many researchers have developed CAD systems for abnormal tissue, tumors, and cancer from a large number of images[7, 8]. The CAD systems assist pathologists in the interpretation of medical images, evaluating the conspicuous structures and supporting a decision-making. Imaging techniques of X-ray, CT, PET, MRI, and bone scan diagnostics yield various types of medical imaging and a large amount of information that the users have to analyze and evaluate. Since every test device uses different criteria and procedure which lead to the variation in values. The images come from different detecting techniques make data analyzing become a difficult task to fulfill. Under the CAD framework, it employs effective image analysis and calculate techniques to process images effectively and evaluate conspicuous sections objectively. It achieved a high-performance level for a computerized diagnosis of cancers in terms of accuracy, speed, and automation. The earlier lung cancer is diagnosed, the easier it is could be better treated[9]. Efforts to improve diagnosis technique and method have not only lead to a greater understanding of the etiology of lung cancer but also increase the patient survival possibilities. The current CAD diagnosis includes Chest X-ray, CT scan, PET scan, MRI and bone scan.

1.3.1 X-ray

An X-ray (CXR) is an imaging test that uses small amounts of radiation to create a two-dimensional image of the organs, tissues, bones and structures inside the chest. Usually, the most common views are taken from posterior-anterior and lateral of patients chest. While X-ray is a relatively cheap tool to investigate diseases of the chest, under some circumstance it is good for screening, but poor for diagnosis. Some lung tumors can be seen by X-ray, other small ones could hide behind the bones and cannot be picked up. Studies estimated that as many as 20-25% of X-ray images are incorrectly interpreted by the pathologists[10].

1.3.2 Computerized Tomography Scan

Computerized Tomography Scan (CT scan), an X-ray equipment linked to a computer combines a series of detailed two-dimensional images taken from different angles to create three-dimensional cross-sectional views of your body parts. Making use of the generated images of the inside body, the pathologist could see and detect the patients blood vessels, bones, and soft tissues without cutting. For the lung cancer, CT scan can be used for detecting both acute and chronic changes in the lung tumors size, location and condition, and the lung cancer metastases. Compared to the traditional plain X-rays, CT scan images provide users more detailed information. Studies have shown that CT improves the detection accuracy of malignancies as 10 times as the X-ray scan do[11].

1.3.3 Positron Emission Tomography

Positron Emission Tomography (PET) is a nuclear imaging technique that detects radiation from the emission of positron-emitting radionuclide (tracer) to observe

biological and metabolic processes in the patients' body[3]. Since cancer cell consumes sugar faster and tends to use more actively energy than a normal cell, it absorbs more radiation. Then, a scanner could detect this substance and create detailed computerized images of the problematic parts of the body. Unlike other imaging techniques, such as X-ray, CT, and MRI, a PET scan could acquire images of physiologic function rather than anatomic function. According to the images which indicate problems at the cellular level, the pathologist could get comprehensive views of systemic diseases, such as lung tumor and cancer spreading.

1.3.4 Magnetic Resonance Imaging

Magnetic Resonance Imaging (MRI) is an imaging technique that uses magnetic field and radio wave energy to generate images of organs and structures inside the body[12, 13, 14]. This radiation-free technique produces images of target areas without using X-ray or gamma ray[15]. For pathologists, MRI has become a method of diagnosing the extent of growth of a tumor and the basis of therapeutic decision-making[16]. However, this scan is rarely used to detect the lungs which move constantly with each respiration. Also, MRI scanner has limited applicability to some patients that have retained pieces of metal in their body.

1.3.5 Bone Scan

Bone Scan is a nuclear medicine imaging technique that helps the user to diagnose and check several types of bone diseases[17]. A bone scan uses a radioactive tracer injected into patients blood vessel to detect the inside of the bones. With its help, pathologists could track bone conditions, such as bone damage, fractures, in-

[3]http://koza.if.uj.edu.pl/files/2dce3ab4e6a6fe76f0ad5fa523de636b/monika_pawlik_seminar.pdf

fection, and inflammation, cancer spreading to the bones and metastasis. Compared to regular X-ray, a bone scan could detect abnormalities days to months earlier.

1.4 Whole Slide Image

Whole-slide image (WSI), which refers to process digital images of an entire microscopic slide to create high magnification digital image being used by a pathologist for diagnosing and research[18, 19, 20]. It makes images easily recognized, increase both the quantity and quality of data obtained from medical images. With integrate images with information systems, applications of whole-slide imaging on histologic image analysis allow the pathologist objectively measures properties of tissue sections and improve diagnostic accuracy and efficiency.

1.4.1 Digital Slide Format

Since WSI is more interactive and easy to share, it is increasingly being used in medical examinations and research. There is some images with different format widely used in the medical practice. The following file formats are supported by the whole-slide image.

1.5 Existing Image Analysis Systems

A multitude of medical image analysis is performed to probe the human body. It applies the image processing and analysis method to the image software to facilitate image interpretation, medical diagnosis, and research. Image software utilized an image viewer which could make users accessible to view, navigate, pan and zoom virtual slides on a digital screen converting the experience of view the traditional

[4]http://free.pathomation.com/

Table 1.1. Type of Microscopic Imaging Data[4]

Format	Image File Extension
TIFF	.tif, .tiff
JPEG	.jpeg, .jpg
JPEG2000	.jp2
PNG	.png
JPEG	.jpeg, .jpg
Olympus VSI	.vsi
Ventana / Roche BIF	.bif
Hamamatsu NDPI	.ndpi
Hamamatsu DICOM	.dcm
Huron Technologies	.tif
3DHistech MRXS	.mrxs
Aperio / Leica SVS	.svs
Leica SCN	.scn
Leica DICOM Sup145	DICOMDIR
Carl Zeiss ZVI	.zvi
Carl Zeiss CZI	.czi
Carl Zeiss Laser Scanning Microscopy	.lsm
Open Microscopy Environment OME-TIFF	.tf2, .tf8, .btf
Nikon ND2	.nd2
Nikon TIFF	.tif, .tiff
Philips TIFF	.tif
Sakura SVSlide	.svslide
Menarini DSight RAW	.ini
Motic	.mds
Zoomify	.zif

light microscopy to a digital format[21]. As introduced on their official website, there are three prevailing image viewers: OpenSlide, ImageJ, and ImageScope.

OpenSlide is a C library that provides users a simple interface to read whole-slide images, which is also called as virtual slides[5].

[5]http://openslide.org/

ImageJ is a public domain, Java-based image processing program for the scientific multidimensional images used in a large scientific user community[6].

ImageScope can open svs image files for review. It supports zooming in/out and annotation of images. Also, this tool can capture interested regions and areas which can be exported as common image formats, such as JPG and TIFF[7].

1.5.1 The Problems and Current Challenges

Large size. Increasing image details and resolution lead to increasing file sizes. The large size of the digital file of gigabits is difficult to store and will be an issue when digitally archive slides. For example, a typical virtual slide with 1,600 megapixels would occupy about 4.6 GB of memory storage[22].

Large RAM. WSI images usually have over exceeded RAM sizes. When the user making uncompressed, it often occupies more gigabytes than other image analysis framework. For example, the open source analysis software ImageJ may fail to open very large virtual slides[23].

Manually labelling ROI. In ImageScope, the pathologists have to control the mouse to draw some areas as ROIs when they carefully view and determine cancer disease. Extra time is cost and attention is also distracted from the valuable work. The time and attention are the precious value for pathologists to do the medical research and determine a cancer disease.

[6]https://imagej.net/Welcome/

[7]https://www.pathology.med.umich.edu/pathology-slide-scanning-service/imagescope-getting-started/

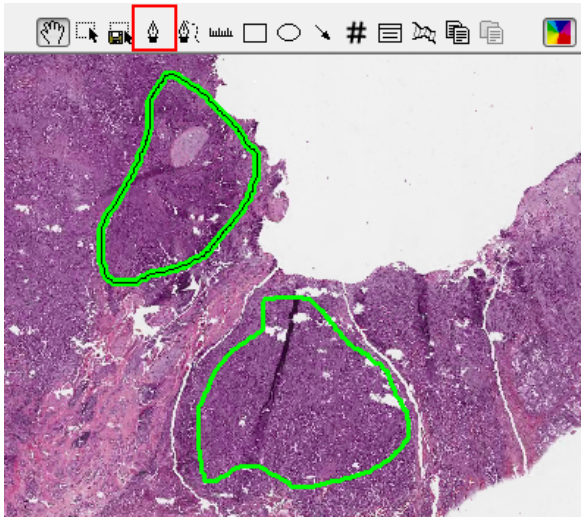

Figure 1.1. ROIs Annotated by ImageScope.

The result of ImageScope is hard to be applied for the future research and education. The output of ROI in ImageScope is an XML file. All coordinate data are recorded in the XML. However, except the coordinate data information, there is not any useful information in the file. In the future, it is impossible to study the experts' behavior by the XML file data.

```
<Annotations MicronsPerPixel="0.503400">
    <Annotation Id="1" Name="" ReadOnly="0" NameReadOnly="0"
        <Attributes/>
        <Regions>
            <RegionAttributeHeaders/>
            <Region Id="1" Type="0" Zoom="0.093944" Selected
            NegativeROA="0" InputRegionId="0" Analyze="1" Di
                <Attributes/>
                <Vertices>
                    <Vertex X="45058" Y="10634" Z="0"/>
                    <Vertex X="45069" Y="10634" Z="0"/>
                    <Vertex X="45122" Y="10634" Z="0"/>
```

Figure 1.2. Output of ImageScope ROI.

1.6 Goal of the Thesis

In this thesis, we proposed a brand new simple CAD system with some new features which benefit to pathologists and pathologists for future research. This new system is named Auto-ROI system.

1.6.1 Automatically Annotate ROI

Supporting manually label ROI is a basic function in the new system. The exciting feature is that the system can automatically detect and save the ROI when pathologists are viewing and trying to determine the cancer disease. Pathologists do not need to draw some areas manually and can pay more attention to the pathological image in the Auto-ROI system.

1.6.2 Apply for The Future Research and Education

Besides the basic coordinate data, the new system gathers and saves all the information related to the pathologists' behavior, such as mouse trace[24], position and the duration of mouse stay, current zoom level and so on. All the above data gathered in the back-end of the system enable us to study the behavior without the guide of a pathologist, even we do not have any medical knowledge background. The more the system record, the more we can get from them. The new system makes it possible for newcomers to grasp how to annotate pathological ROI by self-study.

1.7 Organization

The rest of this thesis is organized as follows. The general background information and knowledge are introduced in Chapter 2. Chapter 3 talks about the overview of the new system. We extend the detailed architecture of the new system in Chapter 4. The whole system architecture and three important modules are investigated.

Theorems of the advantages of forest sparsity are developed. We also discuss several potential applications of forest sparsity. In Chapter 5, a serial of experiments is set up to evaluate the performance of the new system. Finally, we conclude the contributions of this thesis in Chapter 6.

CHAPTER 2

Background

2.1 Introduction

The idea and methodology of the new system is inspired by the Bing Maps Tile System. This chapter will investigate the benefit of the Bing Maps Tile System in a hierarchical file structure.

2.2 Bing Maps Tile System

Bing Maps provides a world map that users can directly manipulate and navigate. To reduce the response time, make fast interaction, and improve the cache ability of request, Bing Maps divides the map into a discrete set of images at many different levels of detail as tiles, cut map into several tiles for fast retrieval and display, then displayed map seamlessly by joining dozens of individual images together and line up properly. Most of these tiles are still displayed relevant and can be kept when the user pan and zoom. The details of Bing Maps are addressed as following, the projection, coordinate systems, and addressing scheme of the map tiles, which is collectively called the Bing Maps Tile System.

2.3 Map Projection: Mercator

To make the map displayed seamlessly on a flat computer screen, Bing Maps uses a single map projection system for the entire world called Mercator. In this way, the whole earth spherical surface is projected into a flat surface. The image below

depicts this concept of Mercator projection which projects spherical earth surface onto a square map.

Figure 2.1. Mercator Projection[1].

2.4 Ground Resolution and Map Scale

In the Bing Maps Title System page, ground resolution means the distance on the ground thats represented by a single pixel in the map. The Bing Maps article also defines the map scale as the ratio between map distance and ground distance in the same units[2].

[1]https://msdn.microsoft.com/en-us/library/bb259689.aspx

[2]https://msdn.microsoft.com/en-us/library/bb259689.aspx/

2.5 Pixel Coordinate

In the Bing Maps, all pixel coordinates for a set of latitude or longitude coordinates on earth can be calculated to (x, y) pixel value on projected square map. As Bing Maps article defines, the upper-left corner pixel of the map is represented by coordinates (0, 0), and the lower-right corner pixel of the map is represented by (width-1, height-1). The calculation of the pixel XY coordinates is:

$$\text{sinLatitude} = sin(latitude * pi/180)$$

$$\text{pixelX} = ((longitude + 180)/360) * 256 * 2^{level}$$

$$\text{pixelY}^{3} = (0.5log((1 + sinLatitude)/(1sinLatitude))/(4 * pi)) * 256 * 2^{level}$$

Bing Maps cut projected map into 256x256 pixel tiles for each zoom level. In this tiling system, the entire world is represented in 4 tiles of 256x256 pixels in the first zoom level. The second zoom level represents the entire world in 16 tiles of 256x256 pixels, and so on. Thus, the higher the zoom level is, the more tiles will be displayed. Quote from Bing Maps Tile System page, as the number of pixels differs at each zoom level, the formula for the number of tiles at each level is:

$$\text{map width}^{4} = \text{map height} = 2^{level} \text{ tiles}$$

[3]https://msdn.microsoft.com/en-us/library/bb259689.aspx/

[4]https://msdn.microsoft.com/en-us/library/bb259689.aspx/

CHAPTER 3

System Overview

This chapter extends to the system overview. It will show what the system looks like and how it works to assist the pathologist in analyzing the cancer disease.

3.1 User Interface

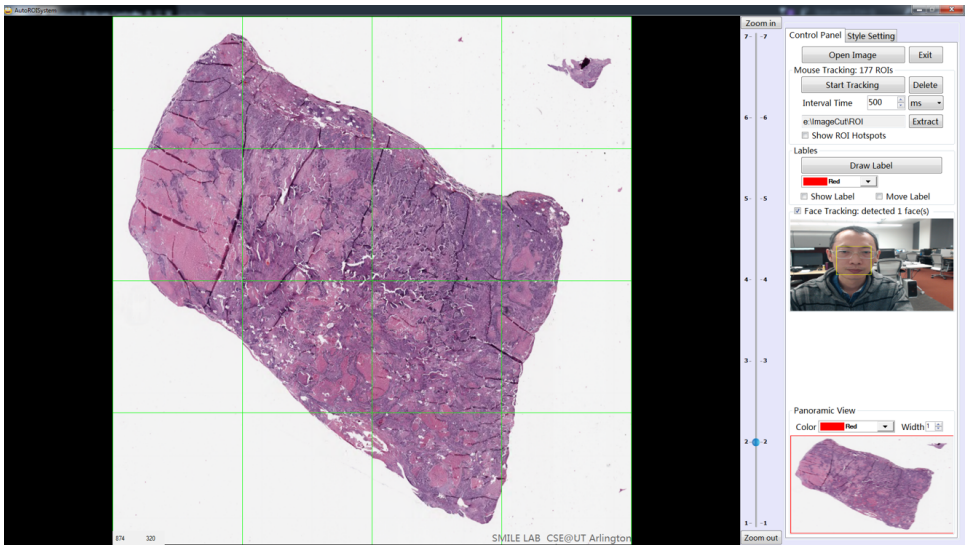

Figure 3.1. User Interface.

There are three main parts in the user interface: display area, control panel, and style setting. The control panel and style setting will be introduced in the next section. In this section, we will focus on the display area. In the Figure 3.1, a whole slide is displayed with the white background. The white area includes 16 cells which are separated by green lines. The Auto-ROI displays 16 tiles instead of the whole

slide or all the tiles. Since most of the whole slide size are over the gigabyte, it is inefficient to load and display the images on a personal computer. Now, displaying the small size patches, which are less than 1M is a high-efficiency alternative solution.

In order to improve the running performance of loading tiles, the Auto-ROI system cache 1,000 tiles in the computer memory to reduce the frequency of accessing the file system. When the users are moving the slide to the right or the left, if the neighbor tiles are caught in the computer memory, the system will firstly accesses the computer memory to get the neighbors. Otherwise, the system will access tile file system on the disk to retrieve them. The tiles cache obviously speed up the access of tiles and reduce the display time. If the PC memory size is large enough, the cache size can be adjusted to buffer more tiles in the memory.

3.1.1 Pan and Zoom

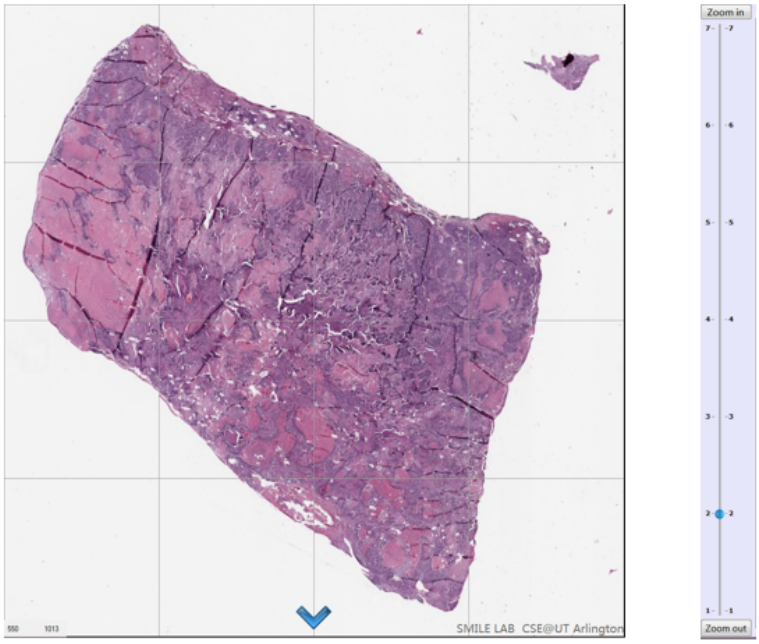

Figure 3.2. Pan and Zoom.

The system enables users to zoom in, zoom out, and pan the slides while they are viewing images. Three ways to zoom the slides are introduced in this system. Double clicking on a specific tile can zoom in the image to the next higher level. Single clicking the zoom bar is the second way to zoom in the image. At last, mouse scroll is the easiest way to zoom in and zoom out any place where the pathologist are interest to view. If the user click the four icons located on the up, bottom, right and left side of white background, the image can be moved to the corresponding direction.

There are 7 different zoom levels are set in the zoom bar. It does not mean that all the slides can be zoomed into the 7^{th} level. What is the highest level the image can be zoomed in depends on the resolution of the image. The higher resolution the image has, the more zoom levels the image has.

3.1.2 Control Panel and Style Setting

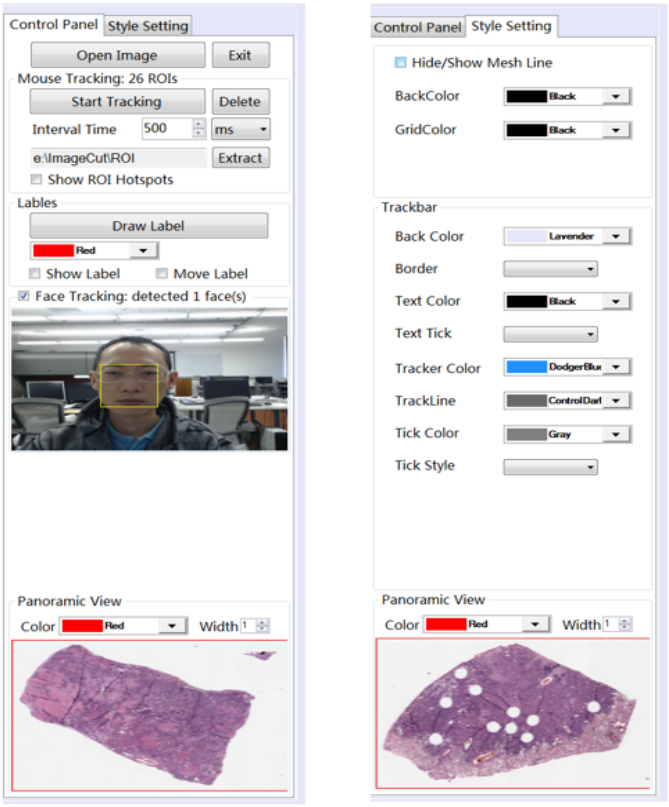

Figure 3.3. Control Panel and Style Setting.

In the control panel, the system provides some functions, such as Open Image, Mouse Tracking, Label ROI, Face Tracking, and Panoramic View, to a pathologist to manage the image. "Open Image" can navigate the user to select the target slide and display it on the screen. In the Auto-ROI system, the target slide is the folder which includes all tiles.

Figure 3.4. Open Image.

In the Mouse Tracking area, clicking "Start Tracking" button will trigger the mouse tracking in the back end. Before the user ends the mouse tracking, a certain mouse trace will be gathered and saved to a database. The precondition is that if the mouse hovers on a position more than the "Interval Time", this position will be tracked to a database. The default value of "Interval Time" is set as 500ms. There are three types of units, millisecond, second, and minute can be set in the Auto-ROI system. Users can freely set the value and time unit according to their behavior habit. If the user select the check box "Show ROI Hotspots", all the positions recorded by system will be shown on the screen. The different spot colors denote different duration of mouse stay. For example, the red color means the longest stay duration, the green color means the shortest stay duration, the blue color means the stay duration between the red and the green[25, 26].

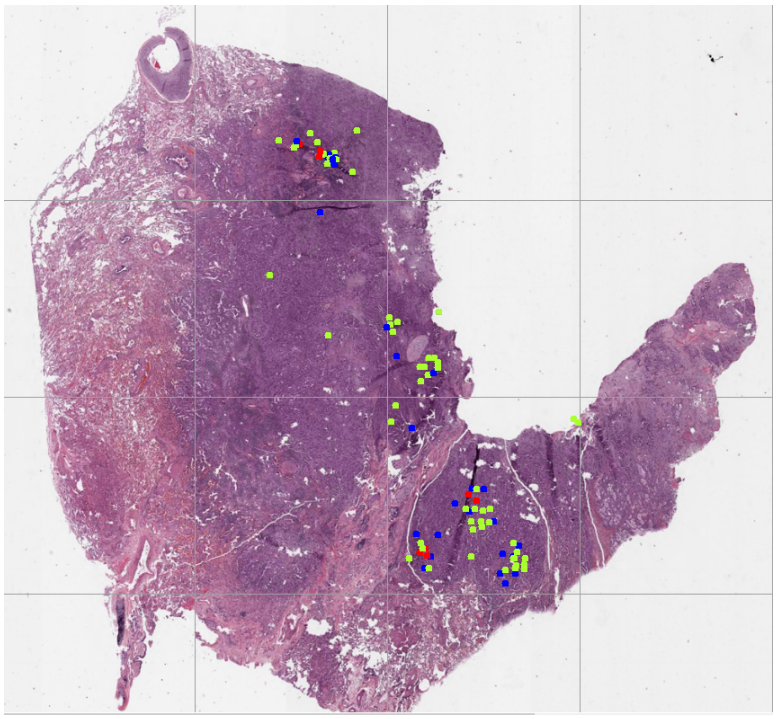

Figure 3.5. ROI Hotspots.

"Draw Label" could make the pathologist to manually annotate a certain area as ROI. This function is kind of similar with ImageScope's related fuction. After clicking the "Draw Label" button, the user move the mouse on the screen and select this area, which includes multiple points. Also, the user can adjust the area by moving point, adding a point, and deleting point.

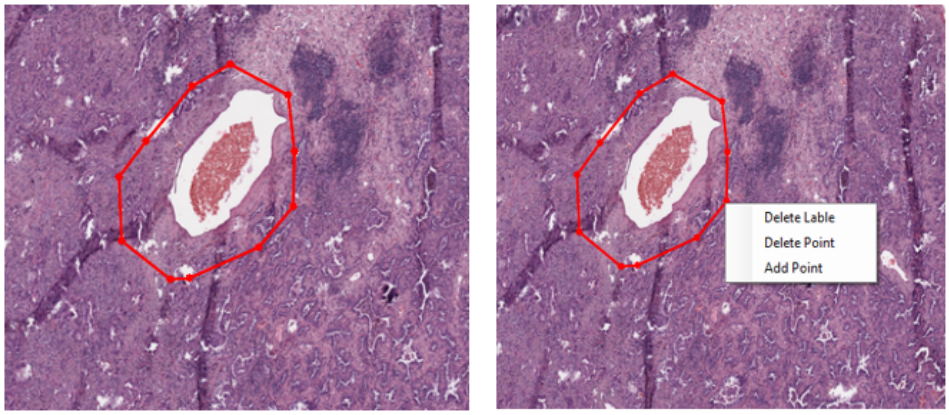

Figure 3.6. Draw Label.

"Face Tracking" is a bright-spot feature in this system[27]. According to this feature, the system can real-time check whether the user is operating the system correctly. What will happen if the "Face Tracking" do not detect any human face? The system will not gather any mouse trace because nobody is detected in front of the computer screen.

Figure 3.7. Face Tracking.

"Style Setting" panel provides a batch of color settings, such as background color, grid color, zoom bar color, zoom bar text color, zoom bar tick color, and so on. This panel provides users more options to choose according to their favorite.

CHAPTER 4

System Architecture and Design

In this chapter, we will introduce the detailed structure of the new system. We also discuss the work process and the business logic in the back end. Finally, three important modules, tile file system, mouse tracking, and face tracking will be analyzed.

4.1 Introduction

Auto-ROI system has some new features created as following. The new system is based on the hierarchical file system, which is not only a source data but also determines the whole system structure, such as query, retrieve, and calculate. Obviously, the system supports the viewing of large SVS slides. Similar to the ImageScope, many regular operations are supported, such as pan, zoom, annotation, and customized setting. The important feature of this system is that it can automatically localize ROI while pathologists are viewing the slides. In order to improve the accuracy of mouse tracking, we also introduce face tracking into this system[28]. The pathologists' detailed behavior information makes it is possible for newcomers to do research and study annotate ROI.

4.2 System Architecture

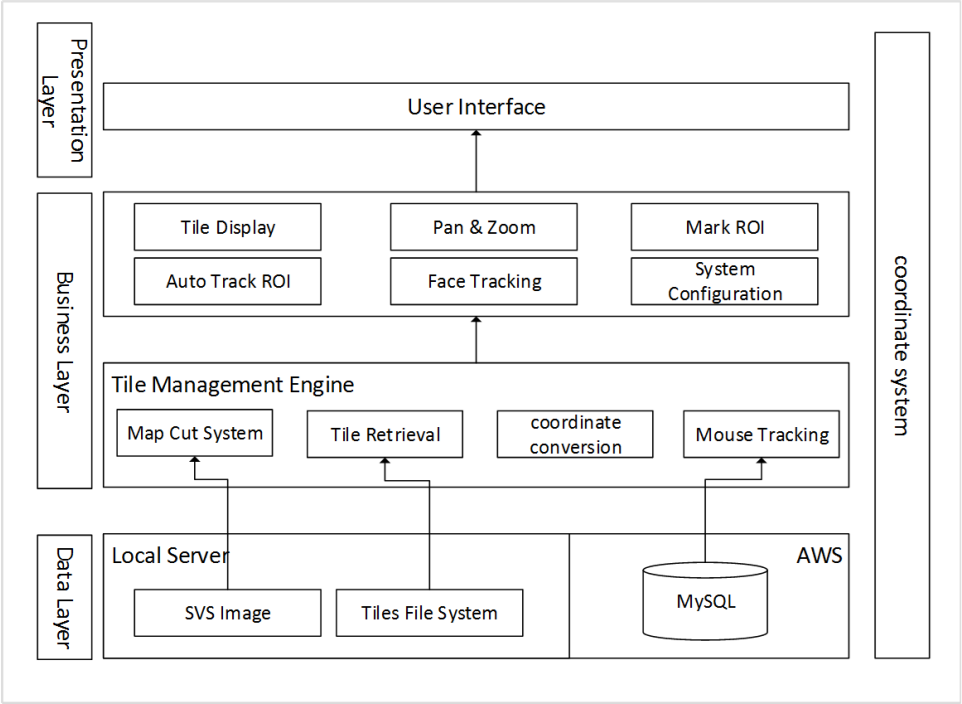

Figure 4.1. System Architecture Diagram.

There are three layers from top to bottom, presentation layer, business layer, and data layer. The user interface and the mouse operation belong to the presentation layer. The business layer deals with all the operations come from the presentation layer, like tile retrieve, display, zoom, tracking and so on. The tile management engine is responsible for map cutting, tile retrieve, coordinate conversion, and mouse tracking. The data layer stores image data into a file system and saves mouse position into a database.

Map cut system is implemented by Python language and utilizes the OpenSlide library. OpenSlide[1] is a open source library which can read whole-slide images by

[1] 1http://openslide.org/

providing useful application interfaces for programmers. Map cut system read regions from the whole-slide image in different zoom level, then resize them to the target tile (256 * 256 pixels).

Tile retrieval module provides the function of querying child tiles, parent tiles or neighbor tiles.

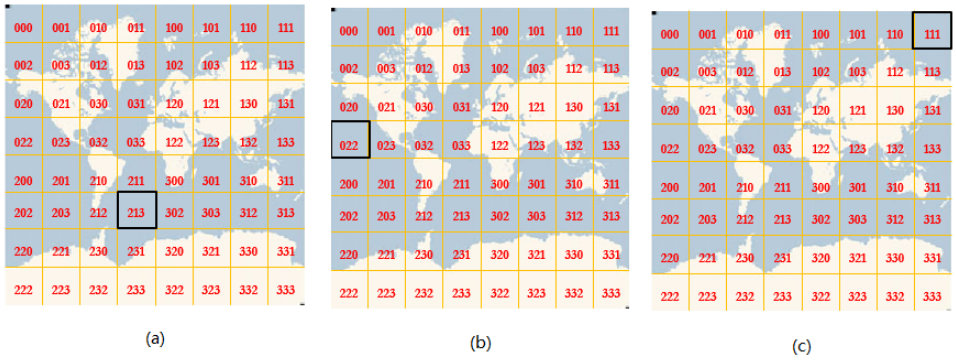

Figure 4.2. Tile Neighbors. (a) Selected tile has 8 neighbors. (b) Selected tile has 5 neighbors. (c) Selected tile has 3 neighbors..

In the center of the new system's display area, most tiles have eight neighbors. However, not every tile has exactly eight neighbors. For example, the tile lies in the four borders has five neighbors[29]. While the tile lies in the four corners has three neighbors. The number variety makes it is hard to display corresponding tiles when a user zooms or pans the image. Every circumstance must be considered in order to retrieve the correct child tiles, parent tiles, and neighbor tiles.

There are some other extreme cases should be mentioned. If the image reaches to its top or bottom, the user could not move up or down anymore. If the slide is already zoomed in to the highest level, the user can't continue to zoom in. In the highest zoom level, all the zoom in operation will be disabled, including double click, zoom bar, and mouse scrolling. It is the corner cases that make the system

complicated in its business logic. When the user moving an image to the left, the system will calculate the number of neighbors. If the number of neighbors is less than eight, the system will consider what other tiles should be included. Also, we should check the value of zoom level in order to determine whether it has parent tiles or child tiles or not.

All the tiles cut from the whole-slide image are stored in the file system, which can be stored both in the local server and remote server. The position information gathered by the mouse tracking is all saved to the MySQL database. In order to improve the usability of the system, the MySQL database is deployed in the Amazon Web Services (AWS). The AWS enables the user to access the position data at any place connected to the Internet. The coordinate system will be introduced along with the mouse tracking module in the next section.

4.3 Tile File System

The original image applied to Auto-ROI system is SVS slide. After cutting the SVS image into small tiles in different zoom levels, the system obtain thousands of tiles. The following example will discuss the tile file system where the system could organize and store these tiles.

The size of a compressed SVS image is 643 MB. After uncompressing the SVS image, the image size increases to 9.0 GB. Generally, the WSI resolution is 1M * 1M pixels, while the image size will be over 40 GB in storage. Base on the Bing Maps Tile System, the WSI is cut and saved to the corresponding folder. When the user zooming and moving the image, the system will directly acquire necessary tiles from the tile file system. Table 4.1 addresses an example of tile number and size in different zoom levels.

Table 4.1. Tile File System Information in Different Zoom Levels

	Number Of Tiles	Number Of Tiles	Size On Disk
Level 1	4^1	4	0.45MB
Level 2	4^2	16	1.71MB
Level 3	4^3	64	7.83MB
Level 4	4^4	256	31.60MB
Level 5	4^5	1024	122.00MB
Level 6	4^6	4096	460.00MB
Level 7	4^7	16384	1,480MB
Total		21844	2.09GB

In the tile file system, the tile name is as same as quadkey. For instance, given tile XY coordinates of (3, 5) at level 3, the quadkey is determined as following.

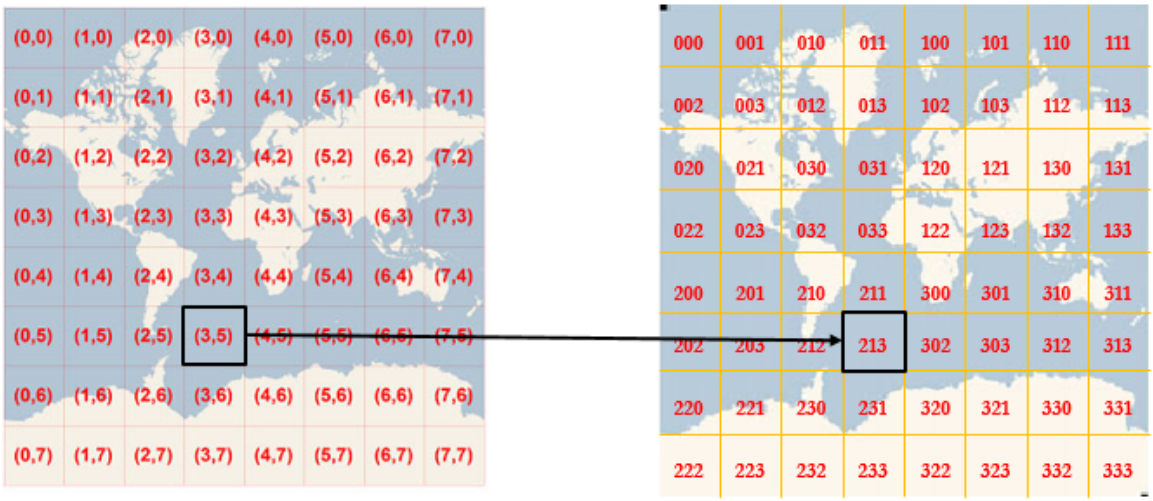

Figure 4.3. Tile Name and Quadkey[2].

[2]https://msdn.microsoft.com/en-us/library/bb259689.aspx

The tile XY coordinates of (3, 5) at level 3 corresponds to the quadkey 213. The next section will discuss the logic method of converting tile XY to quadkey and converting Quadkey to tile XY.

In the local server, the tiles are stored as the following storage structure. All tiles at different zoom levels are collected in the folder, which represents the SVS images individually.

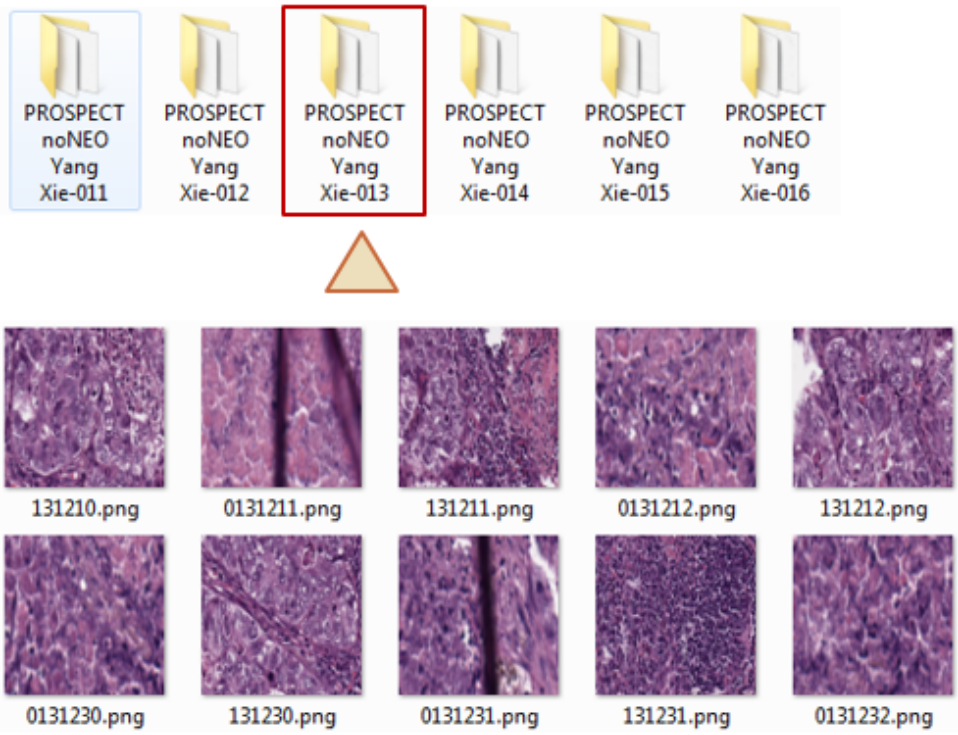

Figure 4.4. File System Structure with Quadkey Filenames.

4.4 Mouse Tracking

In this module, there are four coordinate systems support the mouse tracking logic. With these four coordinate systems, the Auto-ROI system can freely convert the computer screen coordinate to the quadkey.

The first one is screen coordinate. When the mouse is moving or clicking, the first coordinate which the system can catch is screen coordinate. The system can't trace the selected tile without knowing the screen coordinate.

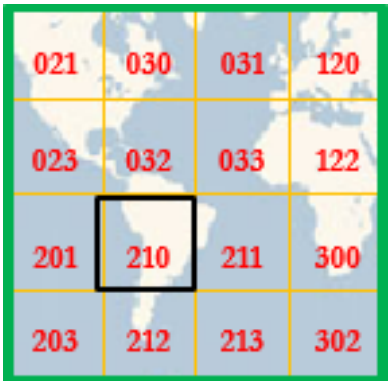

Figure 4.5. Screen Coordinate.

If the 16 tiles in the green square are displayed on the computer screen and the mouse is hovering on a certain tile, which tile is selected depend on the screen coordinate. The 16 tiles belong to 16 grid cells separately. Each grid cell records the corresponding tile information, such as the tile name, the tile size, and the source path. Converting the screen coordinate to the grid cell, the system could calculate and get the selected grid cell. Then, the related tile information is easy to obtain. Finally, the quadkey 210 can be caught from the tile name.

The second one is quadkey. There are some important properties about the quadkey. 1. The length of a quadkey (the number of digits) is equal to the zoom level, at which the corresponding tile locate. 2. The quadkey of parent tile is the prefix of its child tile name. The Figure 4.6 demonstrates that the parent tile quadkey "2" is the prefix of children tile quadkey "20", "21", "22", and "23". Here is the sample code for converting QuadKey to Tile XY coordinates.

Algorithm 1 QuadKey To TileXY

input: quadKey, tileX, tileY, levelOfDetail.

1)$tileX = tileY = 0$;

1)$levelOfDetail = quadKey.Length$;;

repeat

3) int $E(mask = 1 << (i - 1))$;

4) switch $E(quadKey[levelOfDetail - i])$,

$case'0' : break$;

$case'1' : tileX| = maskandbreak$;

$case'2' : tileY| = maskandbreak$;

$case'3' : tileX| = maskandtileY| = mask; break$;

until Stop criteria

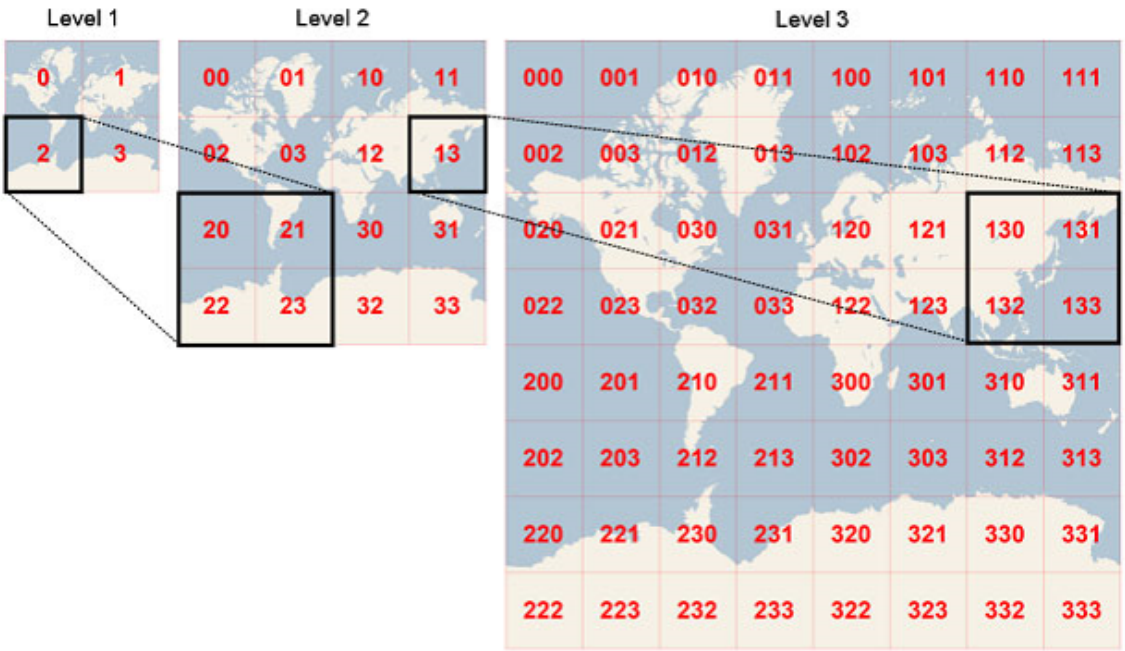

Figure 4.6. Quadkeys Properties[3].

According to the three properties, it is possible to calculate the parent tile or child tile according to the tile name.

The third one is Tile XY Coordinates. Each tile is given XY coordinates ranging from (0, 0) in the upper left to $(2^{level}1, 2^{level}1)$ in the lower right. For example, the tile coordinates range from (0, 0) to (7, 7) at level 3 as following:

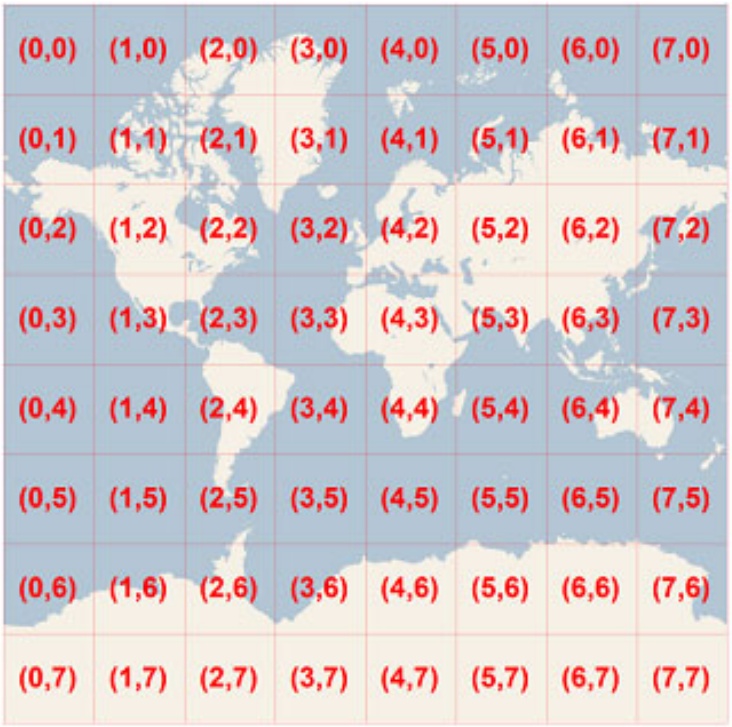

Figure 4.7. Tile XY coordinates[4].

How can the tile XY coordinates be converted to quadkey? To convert a tile coordinates to a quadkey, the bits of the Y and X coordinates are interleaved, and the result is interpreted as a base-4 number.

[3]https://msdn.microsoft.com/en-us/library/bb259689.aspx

[4]https://msdn.microsoft.com/en-us/library/bb259689.aspx

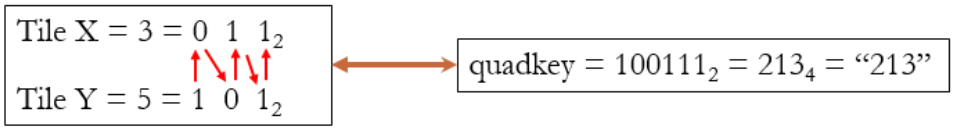

Figure 4.8. Tile XY to Quadkey.

Take the tile XY (3, 5) as an example, the binary value of X is 011 and the binary value of Y is 101. We append the first character of X to first character of Y, to the first character of second Y, then to the first character of second X, and so on. The new binary value 100111 is generated. Finally, the new binary value is converted to base 4 value 213. The final base 4 value is the target quadkey. This is the conversion logic between the tile XY and the quadkey. Here is sample code to implement this conversion.

Algorithm 2 TileXY To QuadKey

input: tileX, tileY, levelOfDetail.

1)$StringBuilderquadKey = newStringBuilder();$

repeat

2)$chardigit =' 0';$

3) int $E(mask = 1 << (i - 1));$

4) If $E(tileX\&mask)! = 0,$

set $digit = digit + 1;$

5) If $E(tileY\&mask)! = 0,$

set $digit = digit + 2;$

until Stop criteria

6)$quadKey.Append(digit);$

The last one is customized coordinates. This coordinate is inspired by the geographic coordinate system. The purpose of using a proper coordinate is recording the real position in the image. The previous three coordinates can't represent the real position of the mouse tracking in the slide. So we introduce a new coordinate to annotate the position. First, we define the coordinate system as two axes and an origin point. The origin point locates to the upper left corner. X axis extends to the right from 0 degree to 180 degree. The Y axis extends to bottom from 0 degree to 180 degree.

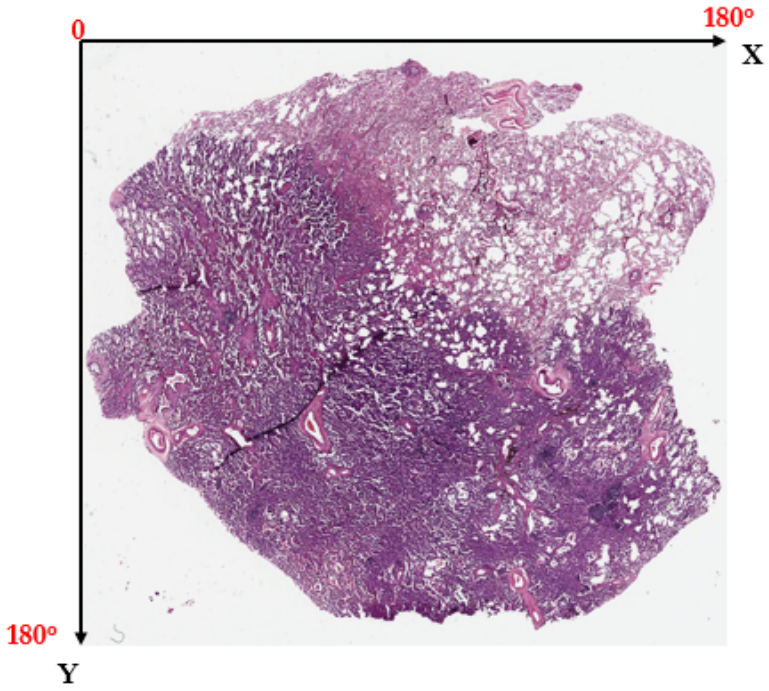

Figure 4.9. Customized Coordinates.

4.4.1 Mouse Tracking Conversion Sample

The above four coordinates system can be converted to each other. The following examples will demonstrate the whole process of conversion.

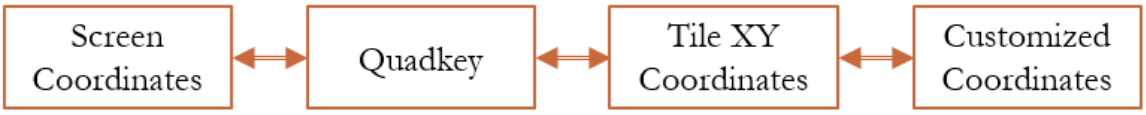

Figure 4.10. Customized Coordinates.

1. Assume the image at zoom level 3 will be shown on the screen. There are totally 64 tiles existed in the file system. Among all the 64 tiles, only 16 tiles can be displayed on the screen. All these 16 tiles locate in the green square of the following image.

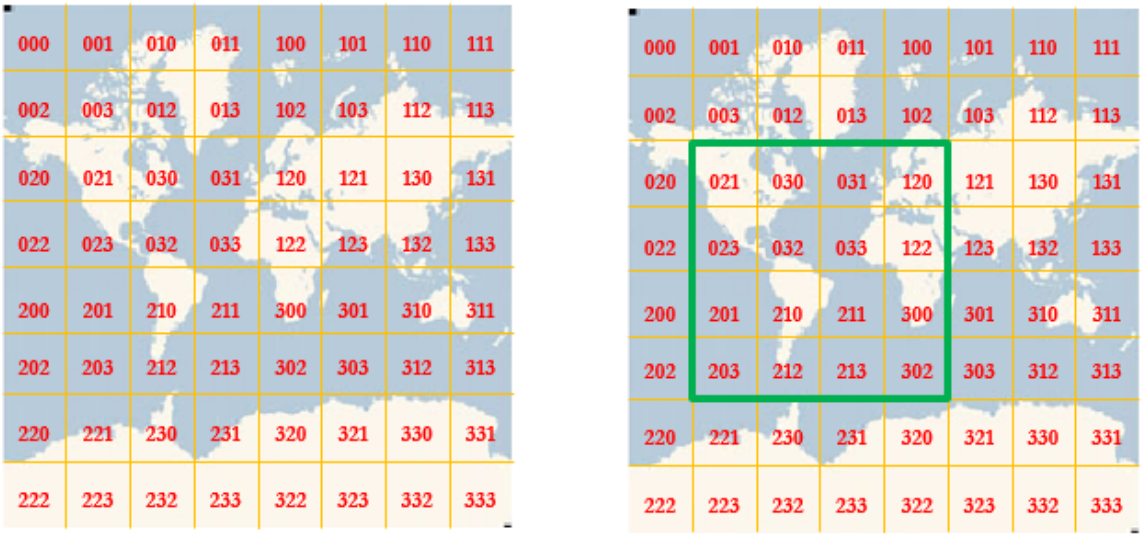

Figure 4.11. Display Area in Level Three[5].

2. Assume the mouse is hovering at the position of (600, 294) in screen coordinate, and the current screen resolution is 1000 * 1000. According to the screen resolution of 1000 * 1000, each grid cell size will be 250 * 250.

[5]https://msdn.microsoft.com/en-us/library/bb259689.aspx

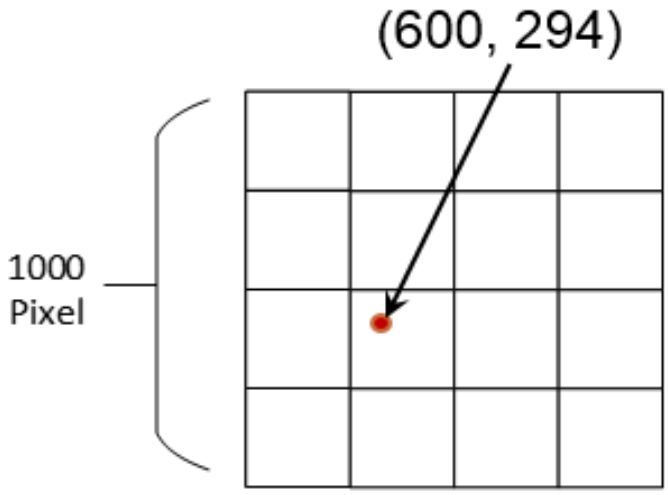

Figure 4.12. Screen Position.

3. The system calculates the grid cell position according to the screen coordinate. The formula of grid cell's position is as following.

grid cell X=600/250=2, grid cell Y=294/250=1.

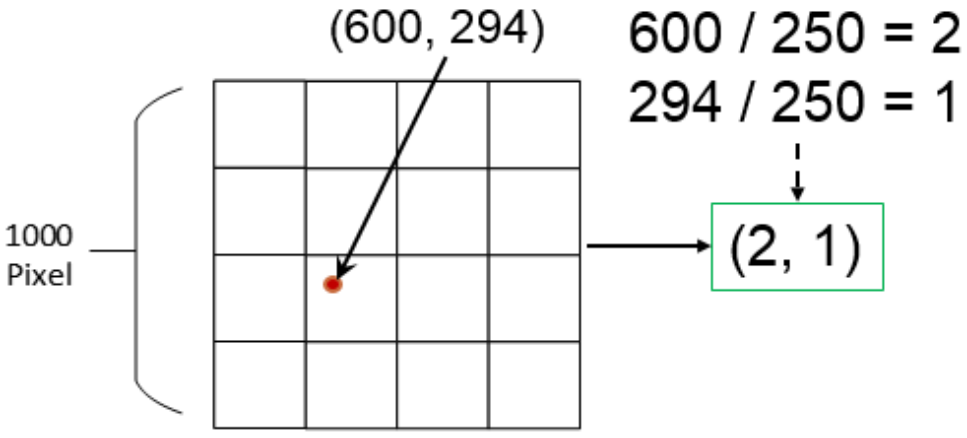

Figure 4.13. Grid Cell Position.

4. From the tile information and grid cell (2, 1), the system could get the tile name as 210.

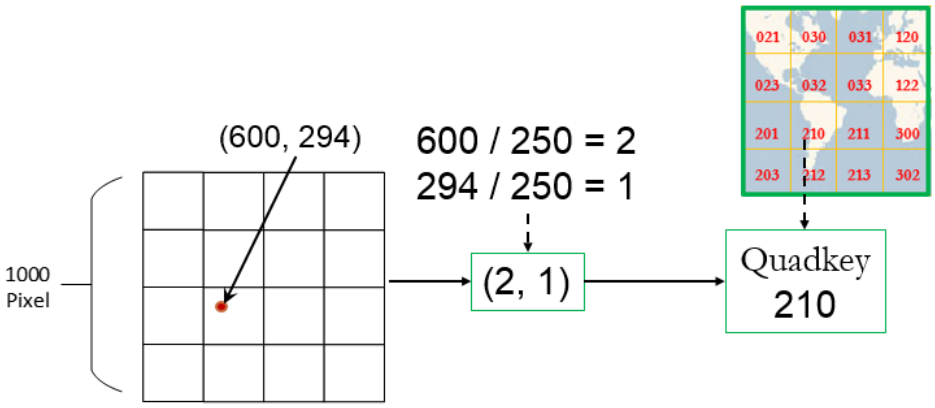

Figure 4.14. Quadkey.

5. Convert quadkey to Tile XY coordinates.

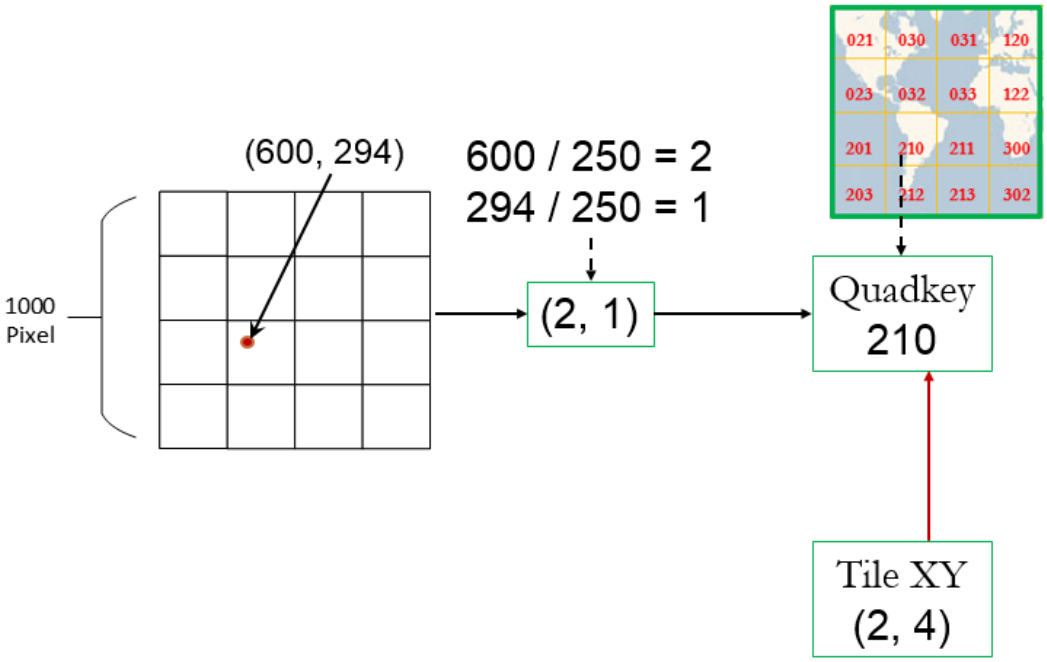

Figure 4.15. Quadkey to Tile XY.

6. Convert tile XY to customized XY. The system projects the whole-slide image to the 180 degree coordinate system. No matter the screen resolution change or not, this image position value is fixed. So this position value is the final result the system need to obtain for the further research.

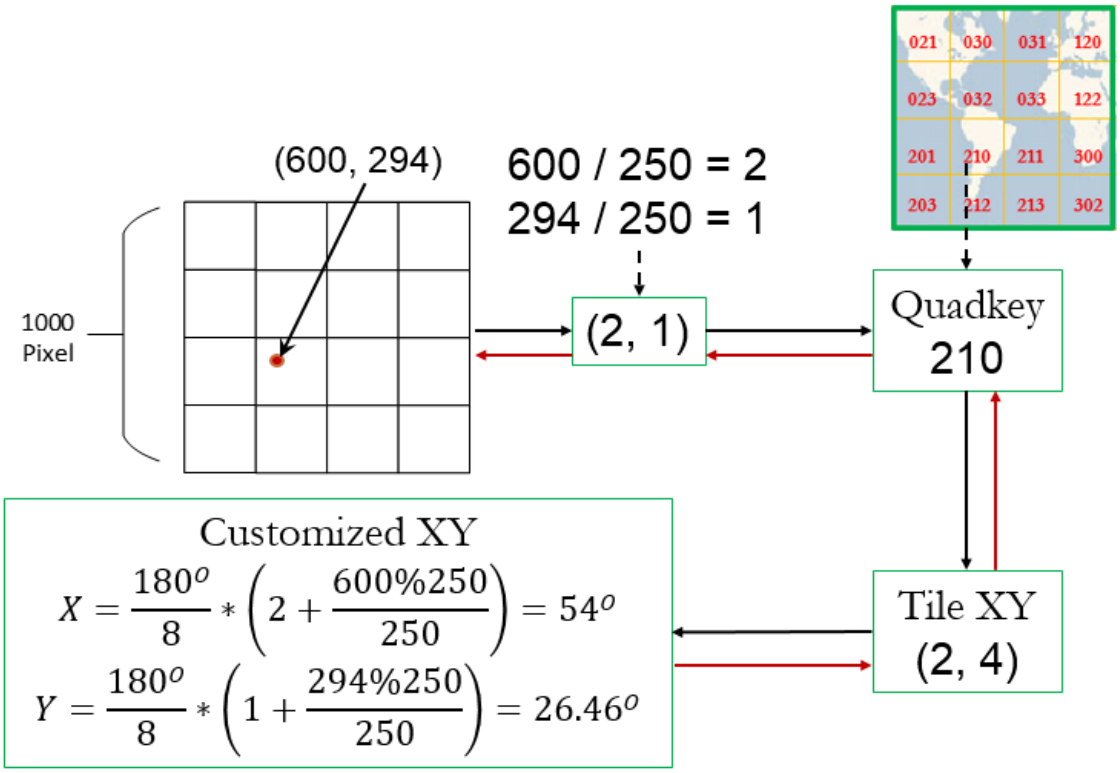

Figure 4.16. Tile XY to Customized XY.

4.4.2 The Comparison with ImageScope

The automatic mouse tracking enables pathologists to focus on the image without distraction from manually labeling ROIs. Here we will compare Auto-ROI with ImageScope, and discuss their performance and properties.

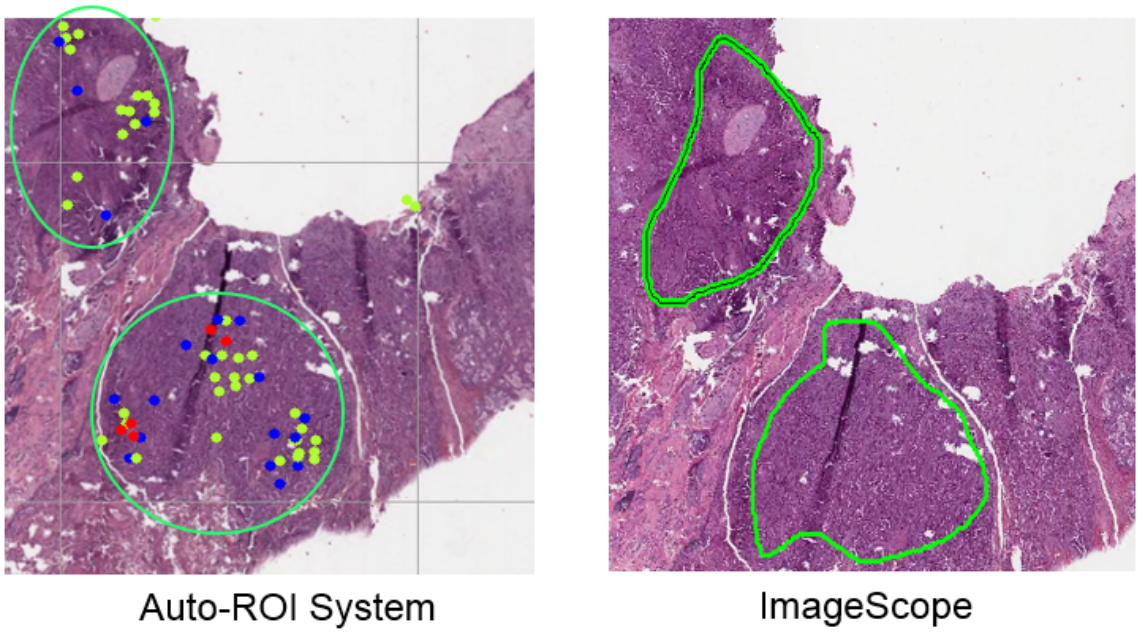

Figure 4.17. Performance Comparison.

To compare their difference, two green areas both in Auto-ROI and ImageScope are marked. As it shows in figure 4.17, the marked two areas are mostly matched. Multiple position points tracked by the mouse are shown in the left "Auto-ROI system". The points density indicates the frequently visited areas which the pathologist viewed the slide. The different color represents the different duration of mouse stay. The concerned area can be predicted for the research by studying the stay duration information. However, the information of point density and stay duration obtained from the Auto-ROI can't get from the ImageScope. Because the ImageScope only records the ROI coordinate without gathering any further data. There is no meaningful information generated in the ImageScope except for the ROI position.

4.5 Face Tracking

In the new system, we also apply face tracking to improve the accuracy of labeling ROI[30]. We assume the pathologist is interested in the colored area in the image to determine the cancer. However, error data localized by mouse tracking is unnecessary and affects ROI accuracy. The face tracking is the method to reduce the error data produced by the mouse tracking. Though the mouse tracking could automatically gather ROI, it has some limitations. From the previous section, we observed that some points are out of the ROI areas in the Auto-ROI system. We call these points as error data because they are not the valid information what the pathologist wants to[31].

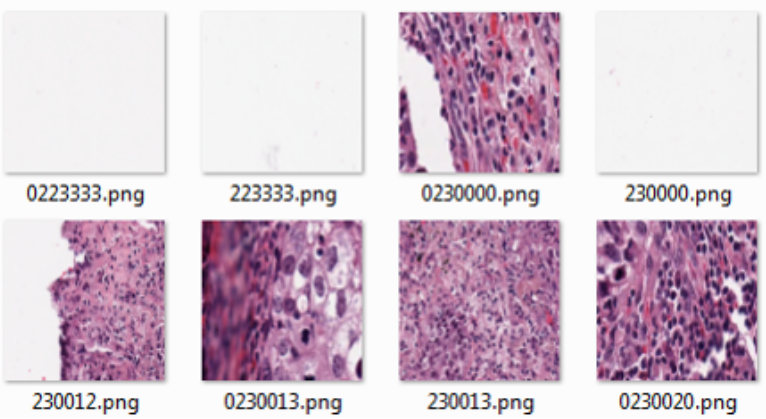

Figure 4.18. Error Data.

As figure 4.19 shows, there are two known scenarios which can cause the error data generated by the mouse tracking.

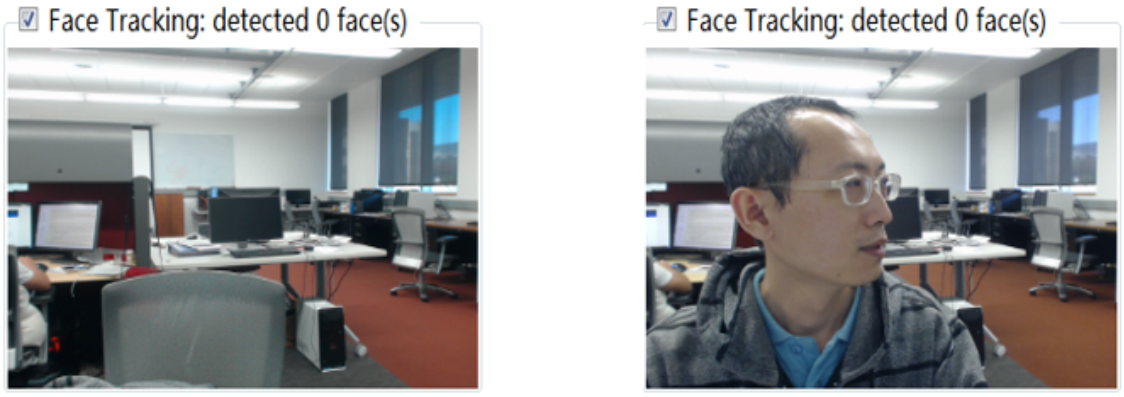

Figure 4.19. Error Data Scenarios. (a) Users leave the seat for coffee without stop mouse tracking. (b) Users move the mouse randomly when talking with others.

The first scenario. As figure 4.19(a) shows, the user leaves their seat to have a cup of coffee or have a rest around without stop using the Auto-ROI. Because in the pathologists' daily work, it is impossible for them to work the whole day without any break. In this case, the system will continue to gather mouse position even though the person doesn't stay in front of the computer screen. There is no doubt that the mouse position is useless[32, 33].

The second scenario. In the figure 4.19(b), the user is talking with other people when he is working. In this circumstance, the user can't view the pathological slide when he is talking to others. However the user still move the mouse without any purpose when he is talking. Eventually, some error data are captured by the system. Maybe there is much more situation which can cause the error data, we will not make examples of them all here.

Since there are many situations could distract user's attention that leads to the error data and less accuracy[34]. We bring face tracking into the system to check

whether the user is really using the system or not. The performance of face tracking is distinctly improved as following.

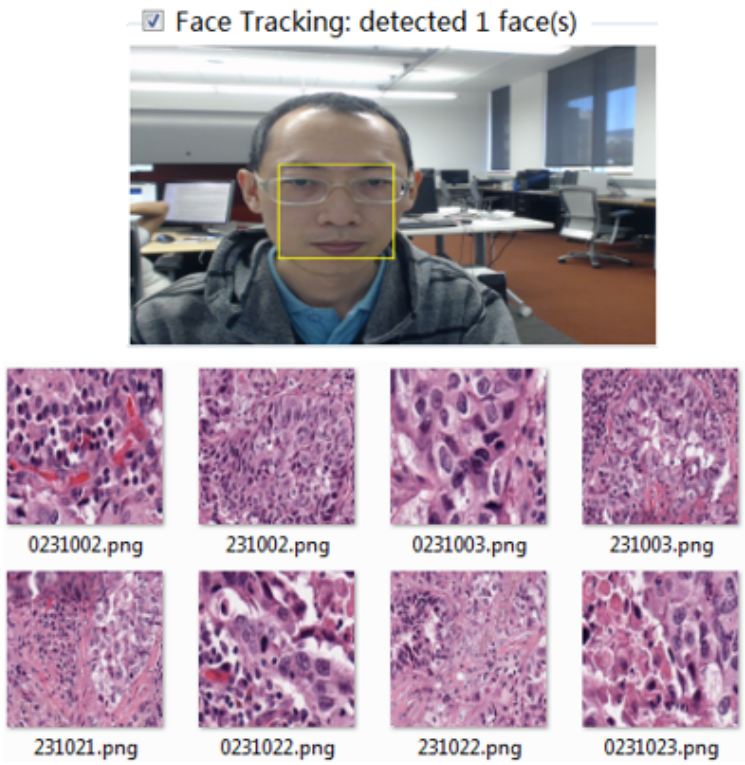

Figure 4.20. Face Tracking.

4.5.1 The Workflow of Face Tracking

There are four preconditions should meet when Auto-ROI capturing a position[35]. Mouse moving is applied; face tracking is enabled; mouse hover on a certain position is over 500ms; at least one human face is detected by the system. If all these four conditions are met, this mouse position will be saved. If any requirement is not met, this mouse position will be ignored. The system checks all of the conditions in the back end of the system in a certain workflow as following.

There are two threads in the system, one is the main thread which controls the whole process of mouse tracking. The other is responsible for controlling web camera and face tracking. These two threads are completely separated to each other.

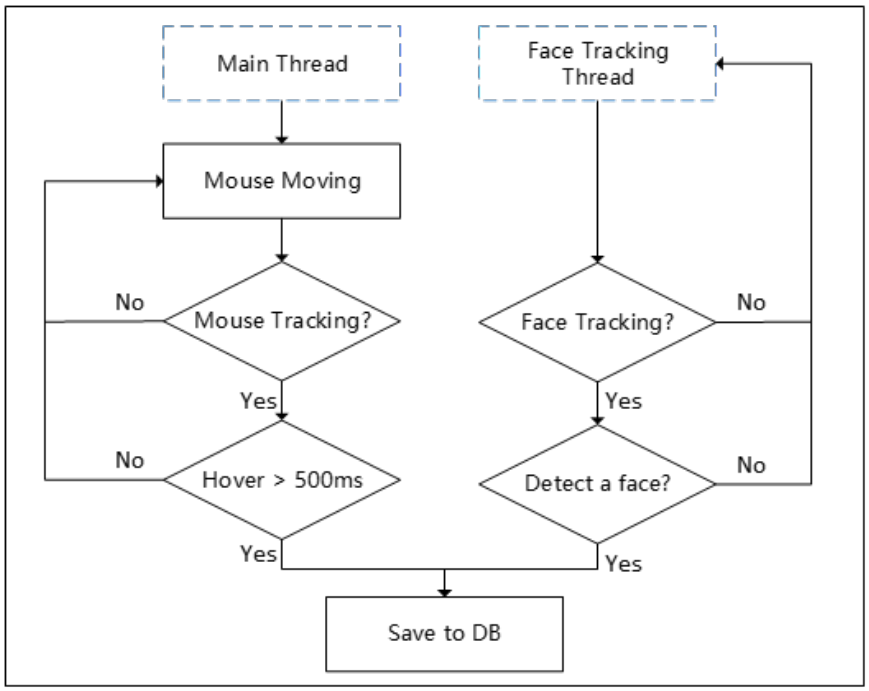

Figure 4.21. Workflow.

4.5.2 The Database Schema

The position data are stored in the MySQL database which is deployed in the AWS. The schema of the data table is shown as following.

Column Name	Datatype	PK	NN
id	BIGINT(20)	☑	☑
point	VARCHAR(1000)	☐	☐
tile_name	VARCHAR(255)	☐	☐
duration	DOUBLE	☐	☐
parent_name	VARCHAR(255)	☐	☐
map_level	INT(11)	☐	☐
create_time	TIMESTAMP	☐	☐

Figure 4.22. The Database Schema.

The sample data in the database is shown as following.

id	point	tile_name	duration	parent_name	map_level	create_time
1116	92.17741,73.46685	1220	664.038	PROSPECT noNEO Yang Xie-016	4	2017-03-30 10:41:25
1117	53.83065,80.30387	0322	576.0329	PROSPECT noNEO Yang Xie-016	4	2017-03-30 10:41:25
1118	58.125,81.79558	0323	856.0489	PROSPECT noNEO Yang Xie-016	4	2017-03-30 10:41:25
1119	86.55241,109.3301	21133	566.0324	PROSPECT noNEO Yang Xie-016	5	2017-03-30 10:41:25
1120	82.01613,109.4233	21132	676.0386	PROSPECT noNEO Yang Xie-016	5	2017-03-30 10:41:25
1121	153.5081,94.59945	3101	777.0444	PROSPECT noNEO Yang Xie-016	4	2017-03-30 10:41:25
1122	164.5161,88.3529	13323	1587.0908	PROSPECT noNEO Yang Xie-016	5	2017-03-30 10:42:19
1123	160.6754,88.41505	13322	869.0497	PROSPECT noNEO Yang Xie-016	5	2017-03-30 10:42:19

Figure 4.23. Sample Data.

4.5.3 The Technique of Face Tracking

In the face tracking module, a web camera is an essential hardware to capture human face. The web camera with higher resolution can improve the accuracy of the face recognition.

EMGU CV is an OpenCV image processing library that is used to implement the face recognition. In the EMGU, the FaceRecognizer is a constructor which enables Eigen, Fisher, and LBPH classifiers to be used together[6].

In order to improve the performance, some techniques are used to improve the performance. The first one is using separated thread to control camera and face tracking in order to avoid the face tracking impact the performance of main thread. The other one is saving position information in batch. Every 50 points will be saved at one time to reduce the frequency of accessing the database.

[6]https://www.codeproject.com/Articles/261550/EMGU-Multiple-Face-Recognition-using-PCA-and-Paral?msg=5388104#xx5388104xx

CHAPTER 5

Experiment and Results

5.1 Dataset Overview

In this experiment, 130 lung adenocarcinoma (ADC) slides are obtained from the University of Texas Lung Specialized Program of Research Excellence (UT Lung SPORE) cohort. All of the 130 slides are from 112 patients.

5.2 Experimental Setup

5.2.1 Configurations

To successfully perform experiments based on the data sets, we set up an environment with the following configuration in SMILE lab.

1. 3.6GHz Intel core i7 4770 CPU with a RAM of memory size 16 GB

2. TACC Stampede System - 4 Compute Nodes (16 cores/node)

The Texas Advanced Computing Center (TACC) is a computing resource deployed in the cloud. The TACC provides some of the most powerful computing resources in the world. The mission of TACC is to enable researchers and scientists to do research through the application of advanced computing technologies[1].

3. Amazon Web Services

Amazon Web Services is a cloud services platform which supports reliable, scalable, and inexpensive cloud computing services.[2]

[1] https://www.tacc.utexas.edu/

[2] https://aws.amazon.com/

Table 5.1. TACC Environment Setup

Component	Technology
Sockets per Node/Cores per Socket	2/8 Xeon E5-2680 2.7GHz (turbo, 3.5)
Coprocessors/Cores	1/61 Xeon Phi SE10P 1.1GHz
Motherboard	Dell C8220, Intel PQI, C610 Chipset
Memory Per Host	32GB 8x4G 4 channels DDR3-1600MHz
Memory per Coprocessor	8GB GDDR5
250GB Disk	7.5K RPM SATA

Table 5.2. AWS Environment Configuration

	Configuration
EngineName	MySQL 5.6.27
License Model	General Public License
DB Name	bigimage
Option Group	default:mysql-5-6 (in-sync)
Resource ID	db-HK3XH3ZBJGU4
Availability Zone	us-west-2a
Publicly Accessible	Yes
EndpointThis	bigimage.c3me4knzxo4d.us-west-2.rds.amazonaws.com
PortDatabase	3306
Certificate Authority	rds-ca-2015
Storage Type	General Purpose (SSD)
Storage	5G
Memory	1G

5.2.2 Software Requirements

1. OS : Windows 7 64 bit, Ubuntu 14.2
2. Programming Languages: C#(.NET Framework 4.0), Python 2.7

5.2.3 Environment Rules

1. Compared with ImageScope

ImageScope[3] is an image viewing application which allows users to load, view, pan, zoom, annotate areas of interests, and analyze slide images taken by the Leica Biosystems scanner.

2. Run both ImageScope and Auto-ROI system in the same environment.

3. Same person annotate the ROI in ImageScope and Auto-ROI system.

4. Applying same rules to determine the ROIs.

5.2.4 Metric

At first, we label 20 slides both in Auto-ROI system and ImageScope separately. Then, we take the ROIs annotated by ImageSCope as ground truth. In this way, the next step is comparing the ROIs labeled by Auto-ROI system with ground truth.

1. Calculate the ratio of ROIs detected by Auto-ROI system belong to the ground truth for each slide.

2. Sum all of the ratios for the 20 slides.

3. Calculate the average ratio for the 20 slides.

The average ratio ranges from 0 to 1. The value closer to 1, the better the result.

5.3 Result Analysis and Conclusion

5.3.1 ROI Coverage

Comparing the ROI areas in Auto-ROI and ImageScope, it is very clear that the areas in both systems are matched. Although the shape of the area is not exactly same because of using the different method to annotate, the approximate outline and position are almost identical to each other. This is the first step to evaluate the result with ground truth.

[3]http://aperio-imagescope.software.informer.com/

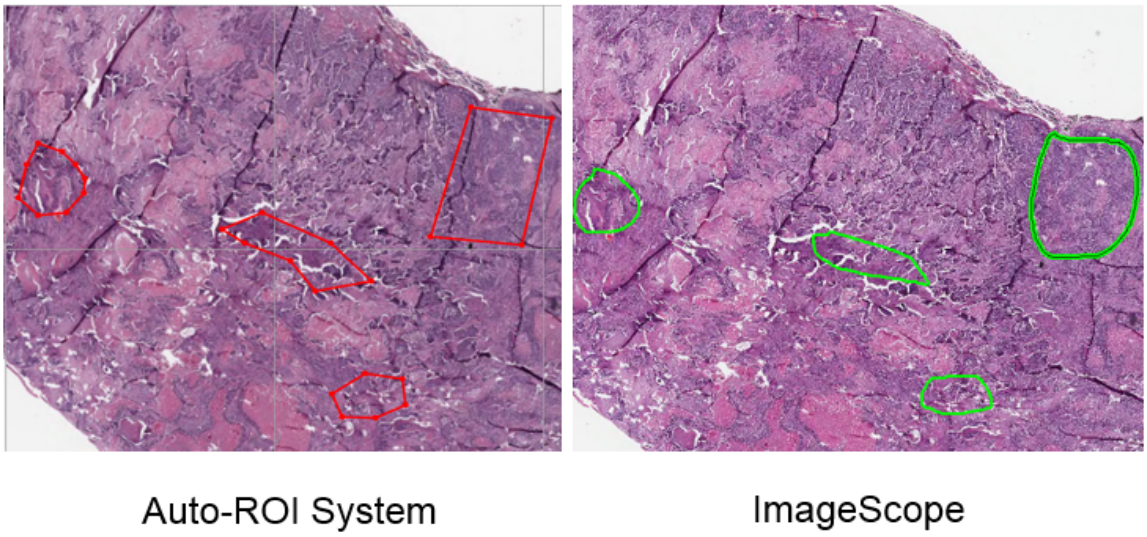

Figure 5.1. ROI Coverage.

Finally, we conclude that the ROI in the new system can fully cover the ground truth.

5.3.2 Accuracy of Mouse Tracking

This is the second step for doing the experiment to evaluate the system accuracy. Now the result of mouse tracking will be compared with the ground truth without the face tracking. Under this circumstance, all of the mouse points will be gathered no matter the user is in front of the computer or not.

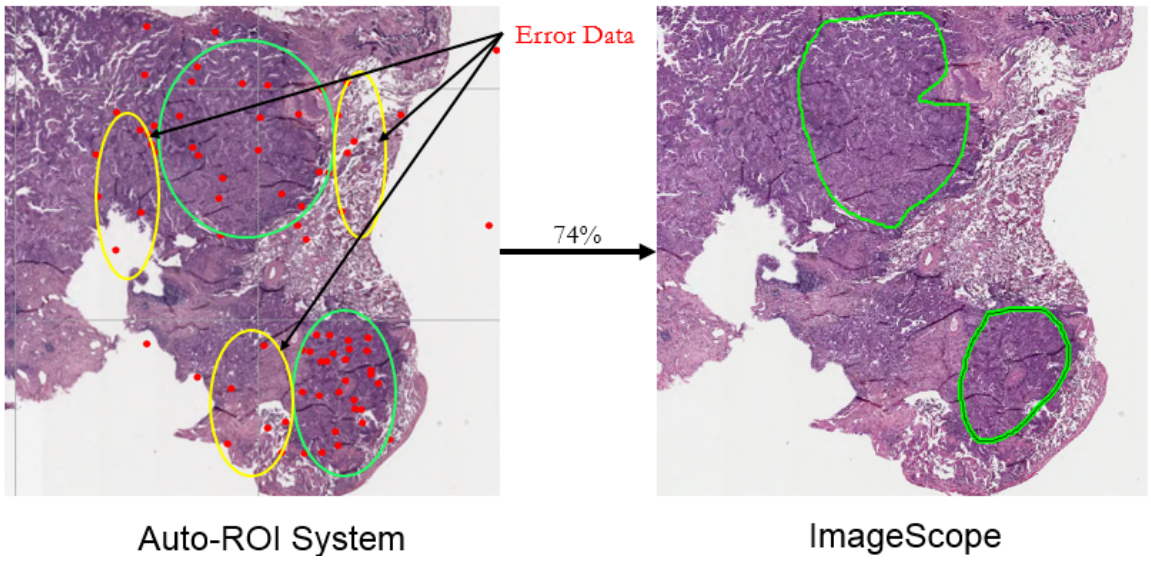

Figure 5.2. Accuracy of Mouse Tracking.

From the above figure, the two green areas in the left image are matched the ground truth in the right image as we discussed in the "ROI Coverage" section. Besides this, there are some points which are surrounded by yellow ellipses. They do not belong to any ground truth data, so we define them as error data. Finally, we get the accuracy of this scenario is 74%, which is lower than what we expected. If the point what we want to gather is only 74 out of 100, the higher possibility for the user to give up the system in the future. That is why we improve the accuracy to assist pathologists to obtain what they want to.

5.3.3 Accuracy of Face Tracking

In this step, face tracking is introduced to compare with ground truth. As we know, the purpose is to reduce the error data and to improve the accuracy of the system. Face tracking is an efficient way to check whether the user is working in front

of the computer by detecting the human face. For the latest version of the system, multiple faces can be detected. While in the future, we can try to identify the right user by recording the user's face image and ignore the strangers' faces.

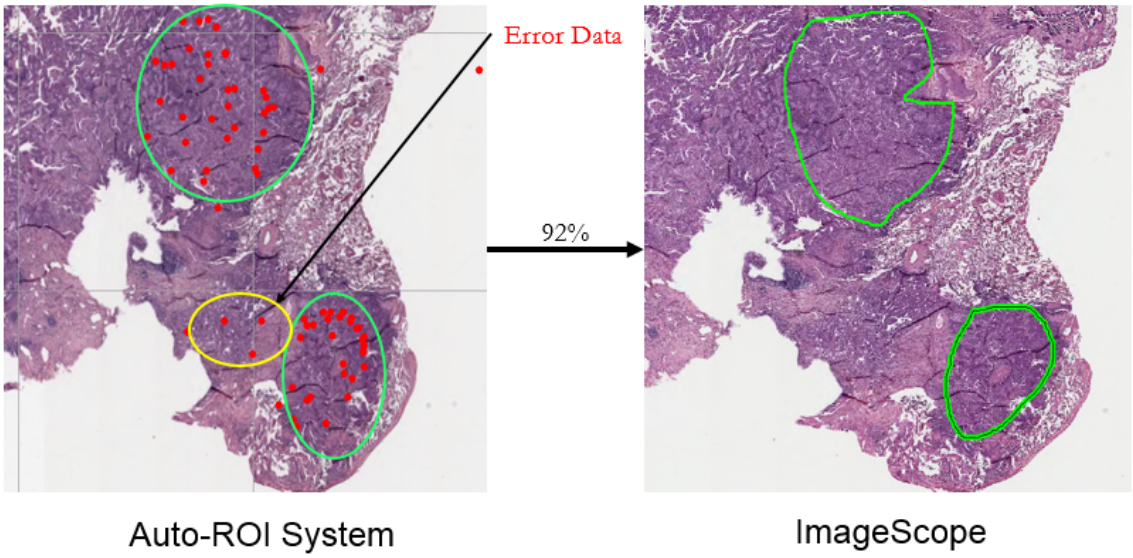

Figure 5.3. Accuracy of Face Tracking.

In this figure, it shows the result of face tracking. It can't be denied that there are still some points which are out of ground truth, the number of error data is increasingly reduced and the accuracy is highly improved from 74% to 92%. This is a really big step for our new system by introducing the face tracking. In this experiment, only 20 slides were labeled and compared. If all of 130 slides are all labeled, we believe the result will be much higher than now.

CHAPTER 6

Conclusion and Future Work

The goal of this thesis is to propose a new CAD system that can apply to the real life to assist pathologists improving the work efficiency and accuracy. The position information outputted by the system can also be applied to the research on studying the pathologists' behavior. It is a prospective and new system because of its higher performance and accuracy that was proven in the experiment. Firstly, the new system supports all basic functions in the ImageScope. That means it will not change users' working habit, such as adjust magnification, pan or zoom, compare different areas, annotate interested areas, and perform image analysis. Secondly, the important feature of the system is no extra time cost brought to the users. Unlike the manual annotation in the Image Scope, the new system automatically tracks, records and saves the region of interest in the back end of the system. It is the new feature that avoids the pathologists distracted from the non-related work. The new feature enables the pathologists to focus on their professional work instead of learning a high-tech software. Thirdly, the new system also demonstrates a high performance and accuracy. Based on the comparison between Auto-ROI and ImageScope in previous experiments, the satisfied result proved that the new system could help the users to accomplish their current work and the future task. Finally, it is a golden opportunity for a researcher to start their analysis on the pathologists' behavior.

Without this new system, it is impossible for newcomers to learn how to annotate ROIs by themselves without the related medical knowledge. For example, if we plan to do an experiment with 1,000 whole-slide images, how can we annotate the

1,000 image before starting the experiment? As a student, it is impossible for us to annotate correctly without any professional training and related medical knowledge. It is unrealistic for a student to determine a lung cancer, breast cancer, and throat cancer through the cancer images. By analyzing the behavior of professional pathologists, a student will learn the method of annotating ROI. This is a big advantage to apply the behavior information to the future research.

There are some areas need to be improved for the new system.

The first, implementation of analyzing behavior data has the highest priority.

The second, implementation of heat map will be introduced to indicate the frequently visited areas.

The third, implementation of eyes tracking will replace the face tracking in order to further improve the accuracy.

The fourth, the usability of the system will be improved.

This is the very beginning of the system, besides the above improvements, we believe the system can achieve higher performance in assisting pathologists.

REFERENCES

[1] R. A. Poldrack, "Region of interest analysis for fmri," *Social Cognitive and Affective Neuroscience*, vol. 2, no. 1, p. 67, 2007. [Online]. Available: + http://dx.doi.org/10.1093/scan/nsm006

[2] R. Li and J. Huang, "Fast regions-of-interest detection in whole slide histopathology images," in *International Workshop on Patch-based Techniques in Medical Imaging*. Springer, 2015, pp. 120–127.

[3] J. Yao, S. Wang, X. Zhu, and J. Huang, "Imaging biomarker discovery for lung cancer survival prediction," in *International Conference on Medical Image Computing and Computer-Assisted Intervention*. Springer, 2016, pp. 649–657.

[4] A. Chapple, S. Ziebland, and A. McPherson, "Stigma, shame, and blame experienced by patients with lung cancer: qualitative study," *bmj*, vol. 328, no. 7454, p. 1470, 2004.

[5] P. van Meerbeeck, Jan, D. A. Fennell, and K. De Ruysscher, Dirk, "Small-cell lung cancer," *The Lancet*, vol. 378, no. 9804, pp. 1741–55, Nov 2011, copyright - Copyright Elsevier Limited Nov 12-Nov 18, 2011; Document feature - Photographs; Tables; Diagrams; ; Last updated - 2015-02-07; CODEN - LANCAO.

[6] M. Anthony J. Alberg, PhD, M. Malcolm V. Brock, M. F. Jean G. Ford, MD, F. Jonathan M. Samet, MD, and M. Simon D. Spivack, MD, "Epidemiology of lung cancer: Diagnosis and management of lung cancer, 3rd ed: American college of chest physicians evidence-based clinical practice guidelines," *Chest*, May 2017.

[7] S. Wang, J. Yao, Z. Xu, and J. Huang, "Subtype cell detection with an accelerated deep convolution neural network," in *International Conference on Medical*

Image Computing and Computer-Assisted Intervention. Springer, 2016, pp. 640–648.

[8] X. Zhu, J. Yao, G. Xiao, Y. Xie, J. Rodriguez-Canales, E. R. Parra, C. Behrens, I. I. Wistuba, and J. Huang, "Imaging-genetic data mapping for clinical outcome prediction via supervised conditional gaussian graphical model," in *Bioinformatics and Biomedicine (BIBM), 2016 IEEE International Conference on*. IEEE, 2016, pp. 455–459.

[9] Z. Xu and J. Huang, "Efficient lung cancer cell detection with deep convolution neural network," in *International Workshop on Patch-based Techniques in Medical Imaging*. Springer, 2015, pp. 79–86.

[10] C. I. Henschke, D. I. McCauley, D. F. Yankelevitz, D. P. Naidich, G. McGuinness, O. S. Miettinen, D. M. Libby, M. W. Pasmantier, J. Koizumi, N. K. Altorki, *et al.*, "Early lung cancer action project: overall design and findings from baseline screening," *The Lancet*, vol. 354, no. 9173, pp. 99–105, 1999.

[11] C. I. Henschke, D. I. McCauley, D. F. Yankelevitz, D. P. Naidich, G. McGuinness, O. S. Miettinen, D. Libby, M. Pasmantier, J. Koizumi, N. Altorki, *et al.*, "Early lung cancer action project: a summary of the findings on baseline screening," *The oncologist*, vol. 6, no. 2, pp. 147–152, 2001.

[12] J. Huang, C. Chen, and L. Axel, "Fast multi-contrast mri reconstruction," *Magnetic resonance imaging*, vol. 32, no. 10, pp. 1344–1352, 2014.

[13] Z. Xu, Y. Li, L. Axel, and J. Huang, "Efficient preconditioning in joint total variation regularized parallel mri reconstruction," in *International Conference on Medical Image Computing and Computer-Assisted Intervention*. Springer, 2015, pp. 563–570.

[14] J. Huang, Z. Qian, X. Huang, D. Metaxas, and L. Axel, "Tag separation in cardiac tagged mri," *Medical Image Computing and Computer-Assisted Intervention–MICCAI 2008*, pp. 289–297, 2008.

[15] J. Huang and Y. Li, *Advanced Sparsity Techniques in Magnetic Resonance Imaging*. Elsevier Press, 2016.

[16] J. Huang, S. Zhang, and D. Metaxas, "Efficient mr image reconstruction for compressed mr imaging," *Medical Image Analysis*, vol. 15, no. 5, pp. 670–679, 2011.

[17] E. E. Kim, "Combined scintigraphic and radiographic diagnosis of bone and joint diseases," *Journal of Nuclear Medicine*, vol. 54, no. 7, pp. 1168–1169, 2013.

[18] X. Zhu, J. Yao, and J. Huang, "Deep convolutional neural network for survival analysis with pathological images," in *Bioinformatics and Biomedicine (BIBM), 2016 IEEE International Conference on*. IEEE, 2016, pp. 544–547.

[19] J. D. Webster and R. W. Dunstan, "Whole-slide imaging and automated image analysis," *Veterinary Pathology*, vol. 51, no. 1, pp. 211–223, 2014, pMID: 24091812. [Online]. Available: http://dx.doi.org/10.1177/0300985813503570

[20] X. Zhu, J. Yao, X. Luo, G. Xiao, Y. Xie, A. Gazdar, and J. Huang, "Lung cancer survival prediction from pathological images and genetic dataan integration study," in *Biomedical Imaging (ISBI), 2016 IEEE 13th International Symposium on*. IEEE, 2016, pp. 1173–1176.

[21] M. G. Rojo, G. B. Garca, C. P. Mateos, J. G. Garca, and M. C. Vicente, "Critical comparison of 31 commercially available digital slide systems in pathology," *International Journal of Surgical Pathology*, vol. 14, no. 4, pp. 285–305, 2006.

[22] S. Park, L. Pantanowitz, and A. V. Parwani, "Digital imaging in pathology," *Clin Lab Med*, vol. 33, no. 4, pp. 557–584, October 2012.

[23] N. Farahani, A. V. Parwani, and L. Pantanowitz, "Whole slide imaging in pathology: advantages, limitations, and emerging perspectives," *Pathology and Laboratory Medicine International*, vol. II, June 2015.

[24] E. Hehman, R. M. Stolier, and J. B. Freeman, "Advanced mouse-tracking analytic techniques for enhancing psychological science," *SAGE*, vol. 18, no. 3, pp. 384–401, May 2015.

[25] J. B. Freeman and N. Ambady, "Mousetracker: Software for studying real-time mental processing using a computer mouse-tracking method," *Behavior Research Methods*, vol. 42, no. 1, pp. 226–241, 2010.

[26] V. Navalpakkam and E. Churchill, "Mouse tracking: measuring and predicting users' experience of web-based content," in *Proceedings of the SIGCHI Conference on Human Factors in Computing Systems*. ACM, 2012, pp. 2963–2972.

[27] S. Petrescu, P. Corcoran, E. Steinberg, P. Bigioi, and A. Drimbarean, "Real-time face tracking in a digital image acquisition device," June 3 2014, uS Patent 8,744,145. [Online]. Available: https://www.google.com/patents/US8744145

[28] J.-Z. Huang, T.-N. Tan, L. Ma, and Y.-H. Wang, "Phase correlation based iris image registration model," *Journal of Computer Science and Technology*, vol. 20, no. 3, pp. 419–425, 2005.

[29] Y. Li, C. Chen, W. Liu, and J. Huang, "Sub-selective quantization for large-scale image search," in *Proceedings of the Twenty-Eighth AAAI Conference on Artificial Intelligence, July 27 -31, 2014, Québec City, Québec, Canada.*, 2014, pp. 2803–2809. [Online]. Available: http://www.aaai.org/ocs/index.php/AAAI/AAAI14/paper/view/8450

[30] X. Chen, C. Zhang, F. Dong, and Z. Zhou, "Parallelization of elastic bunch graph matching (ebgm) algorithm for fast face recognition." in *ChinaSIP*, 2013, pp. 201–205.

[31] M. Kim, S. Kumar, and V. Pavlovic, "Face tracking and recognition with visual constraints in real-world videos," in *Computer Vision and Pattern Recognition*. Anchorage, AK, USA: IEEE, June 2008.

[32] G. Bradski, "Real time face and object tracking as a component of a perceptual user interface," in *Applications of Computer Vision, 1998*. Princeton, NJ, USA: IEEE, October 1998.

[33] X. Chen, C. Zhang, and Z. Zhou, "Boosting non-graph matching feature-based face recognition with a multi-stage matching strategy," *International Journal of Wavelets, Multiresolution and Information Processing*, vol. 15, no. 02, p. 1750017, 2017.

[34] G. Wang, M. Z. A. Bhuiyan, J. Cao, and J. Wu, "Detecting movements of a target using face tracking in wireless sensor networks," in *IEEE Transactions on Parallel and Distributed Systems*, vol. 25, no. 4. IEEE, April 2014, pp. 939 – 949.

[35] J. Shen, S. Zafeiriou, G. G. Chrysos, J. Kossaifi, G. Tzimiropoulos, and M. Pantic, "The first facial landmark tracking in-the-wild challenge: Benchmark and results," in *Computer Vision Workshop (ICCVW)*. Santiago, Chile: IEEE, December 2015.

BIOGRAPHICAL STATEMENT

Shirong Xue was born in Shanxi, China. He received the B.E. degree in Computer Science from Shanxi University, Shanxi, China in 2003. He has been a graduate student in the Department of Computer Science and Engineering at the University of Texas at Arlington since 2015. His major research interests include machine learning, image processing, and computer vision. He also has over 10 years work experience as software engineer in the IT industry. He has been involved in multiple large enterprise level and highly distributed system. His years of work experience in scrum methodology, test-driven development, and continuous deployment enable him to utilize his technical skills, organizational skills and academic background to a real software project.